Florian Feyersinger Bsc

Simulation of Ion Movement in Barium Lithium Fluoride

MASTER'S THESIS

to achieve the university degree of

Diplom-Ingenieurin

Master's degree programme: Technical Chemistry

submitted to

Graz University of Technology

Supervisor

Univ.-Prof. Dr. A. Daniel Boese

Graz, August 2018

AFFIDAVIT

I declare that I have authored this thesis independently, that I have not used other than the declared sources/resources, and that I have explicitly indicated all material which has been quoted either literally or by content from the sources used. The text document uploaded to TUGRAZonline is identical to the present master's thesis.

Date

Signature

II

Contents

List of Figures

List of Tables

0.1 Abstract

Nowadays, the demand for newer and better materials in a huge variety of fields of applications is extremely high. One such field is the battery industry [1, 2, 3]. Promising materials in batteries are for example solid electrolytes.
One way in effectively finding and developing new materials is in understanding the basic principles behind the occurring electrochemical processes.
Experimental analysis of samples are most of the time not sufficient enough for a complete understanding of the involved processes and for that reason, simulations are needed. In this thesis, the ion movement in a solid crystal will be simulated via calculation of the energy barrier the ions have to overcome by changing position in the crystal lattice.
The calculations will be done with the Vienna ab initio Simulation Package (VASP) and the results will be compared to experimental data from impedance measurements.
The simulated material is Barium Lithium Fluoride. $BaLiF_3$ is known as ion conductor, the conduction can be separated in Li^+ as well as F^- conduction both with unknown pathway, especially since Li^+ may occupy a Ba^{2+} lattice position and vice versa.
The goal of this thesis is to calculate the different ion conduction pathways to find the most likely conduction mechanism for both conducted-species.

0.2 Kurzfassung

Batterien finden heutzutage in vielen Geräten als Energiespeicher Verwendung und dadurch wächst das Bedürfnis nach neuen und möglicherweise besseren Materialien für Batterien [1, 2, 3], wie zum Beispiel Festkörperelektrolyte. Ein wichtiger Schritt um neue Materialien zu finden und zu entwickeln, ist es die zu Grunde liegende Theorie zu verstehen.

Dadurch, dass Experimente zu meist nicht ausreichend Daten für vollständige Theorien liefern, ist es notwendig, Simulationen durchzuführen. In dieser Arbeit werden Berechnungen von Energiebarrieren bei der Bewegung von Ionen innerhalb eines Kristallgitters durchgeführt.

Diese Berechnungen werden mit dem Vienna Ab Initio Simulation Package (VASP) gemacht und die erhaltenen Ergebnisse werden, mit davor durchgeführten Impedanz-Spektroskopie Messungen verglichen.

Das hier untersuchte Material ist Barium Lithium Fluorid. $BaLiF_3$ ist als Ionenleiter bereits bekannt, innerhalb dieses Materials soll es F^- und Li^+ Leitungen geben, aber es konnte bisher nicht klar festgestellt werden, welchen Weg die jeweiligen Ionen zurücklegen, insbesondere da Lithium auch die Kristallgitterposition von Barium einnehmen kann und umgekehrt.

Das Ziel dieser Arbeit ist es die verschiedenen möglichen Wege der Ionen in $BaLiF_3$ zu simulieren und dadurch den am wahrscheinlichsten für beide Ionen zu finden.

Introduction

1.1 Basics on ion movement in solid state and cristallography

A crystal is a solid material containing atoms or molecules which are arranged in a highly ordered structure, the crystal lattice. This lattice can be reproduced by repeating a small amount of particles in a defined arrangement various times. The smallest possible arrangement needed for lattice reproduction is the unit cell.
An assembly of unit cells can create a repeating unit which may also describe the crystal.
Super cells are cells containing more than one unit cell and are used for bulk simulations. For example, a super cell could be containing 125 unit cells (5 in each dimension), an example with a 2x2x2 super cell compared to the unit cell is given in Figure 1.1.

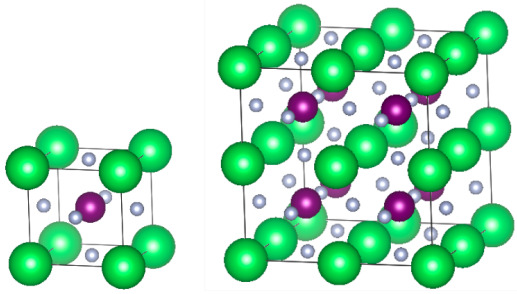

Figure 1.1: unit cell and super cell
left unit cell, right 2x2x2 super cell of $BaLiF_3$.

Ions can move via change of one lattice position to another lattice position which was empty before, visualized in Figure 1.2. This model will be used to describe the ion transport in solid state in this thesis. Another possibility for ion movement is also visualized in Figure 1.2 in green, interstitial sites are positions in between the lattice positions, ions may move from one interstitial site to another. This mechanism will not be calculated in this thesis.

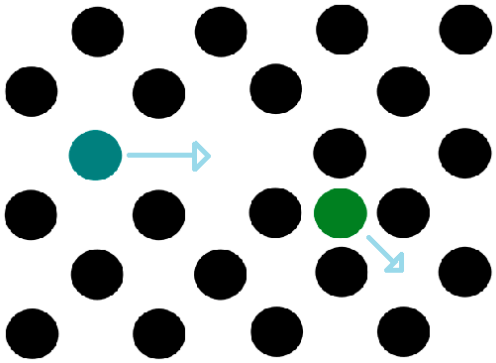

Figure 1.2: ion transport mechanism
blue ion: vacancy mechanism for ion diffusion as used in this thesis, green ion: ion jump from one interstitial site to another.

Empty lattice positions are called point defects. There is a variety of different possible defects in solids like line, point and screw defects. In this work the point

defects are the most important type. Point defects can be further categorized into Schottky and Frenkel defects.

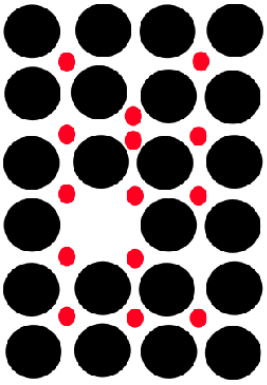

Figure 1.3: different defects
Schottky defects on the bottom, with one missing black and one missing red particle. Frenkel defects on top of the figure, with one red particle moving to another interstitial position.

Frenkel defects are described by the position change of one atom from a lattice position to an interstitial lattice position, as pictured in Figure 1.3, which leaves a vacancy on the previous position of the atom, represented in Equation 1.1.

$$M_M^x \rightarrow V_M + M_i \tag{1.1}$$

The Frenkel defect equation follows the so-called Kroeger-Vink notation. M_M^x is an atom of element M without relative charge at the lattice position of M. V_M is a vacancy with a single negative relative charge at a M-lattice position and M_i is an atom of element M with a single positive relative charge positioned at an interstitial site.

In Schottky defects, atoms are leaving the material completely, leaving vacancies behind, as shown in Figure 1.3 and Equation 1.2 those atoms that left the material

may create other components.

$$M_M^x + A_A^x \rightarrow V_M + V_A^{\cdot} + MA \tag{1.2}$$

Schottky defect equation,A_A^x represents an atom of element A without relative charge in a lattice position of A. $V_A^{\cdot}$ is a vacancy with positive relative charge at the lattice position of A and MA is a additionally formed material or molecule.

The calculation done in this thesis will only be based on Schottky defects and their contribution to the ion movement in solid material. Therefore no interstitial sites, which are only used in Frenkel defects, will be calculated as starting points for the ion transport.

The formed extra material has to be energetically compensated in the defect building energy (E_{db}), this formalism will be discussed in section 1.2.

In a perfect crystal there are no defects, but in real crystals there is always a small amount of them. The number of defects in a crystal lattice is dependent on the available energy and therefore, on the temperature of the system and the energy needed to form such defects. This relation is represented in Equation 1.3.

$$N_{defect} = N_{atom} * e^{\frac{-E_{db}}{k*T}} \tag{1.3}$$

Relation of the number of defects to temperature. N_{defect} is the number of created defects. N_{atom} is the total number of atoms. E_{db} is the defect building energy. k represents the Boltzmann constant and T is the temperature

One important parameter for ion movement is the defect concentration in the material. This concentration gives the ratio of point-defects to the number of total atoms and is therefore always below 1 as seen in Equation 1.4. The defect concentration is important since different concentrations may influence the energy barrier and/or the defect formation energy. The definition of defect concentration ins given in Equation 1.4.

$$c_{defect} = \frac{N_{defect}}{N_{atom}} \tag{1.4}$$

defect concentration c_{defect} with N_{defect} as the number of defects and N_{atom} as the total number of atoms in the system

Calculations in this thesis are, in the first step, done at 0 K with some manually created defects since they are needed for ion conduction. After the first calculations a combination of the programs Phonopy with VASP, in case of the unit cell itself and additional calculations only with VASP but other INCAR input (specifics in chapter 2) in case of bigger cells, will be used to simulate higher temperature in form of the harmonic oscillator approximation. This type of calculation is needed since higher temperatures create oscillating atoms in the lattice and may in- or decrease the energy barrier for the ion movement [4].

1.2 Background of Ion Movement and Density Functional Theory (DFT)

1.2.1 Ion movement

Defects have a formation energy to overcome. The defect formation energy is given by Equation 1.5:

$$E_{db} = E_{defs} - E_{perfs} + E_{molecule} \tag{1.5}$$

E_{db} is the defect formation energy. $E_{perfs}$is the energy of the system without any defects. E_{defs} is the energy of the system with one defect and $E_{molecule}$ is the energy obtained by forming possible molecules or material out of the atoms creating the defect as mentioned in section 1.1

To obtain the energy barrier of the ion movement a rather simple equation can be used:

$$E_{barrier} = E_{defs} - E_{trans} \tag{1.6}$$

$E_{barrier}$ is the energy barrier which needs to be overcome for ion movement and E_{trans} represents the energy of a transition state

This transition state needed for Equation 1.6 will be introduced by placing an atom on a position in the material which is in-between two optimized lattice positions, a similar case is represented in Figure 1.4.

Figure 1.4: transition state
left: starting point in optimal lattice position, middle: transition state the lattice may be disturbed, right: end point again in optimized lattice position.

This creates an image of a moving atom from one lattice position to another.The nudge elastic band script (NEB-script) in VASP will be used to find the maximum energy barrier, see subsection 1.4.1, since we are only interested in the highest energy. In-between those empty lattice positions there may exist more than one saddle point, see section 4.2. The position of this saddle points are unknown at the beginning.

1.2.2 Introduction of molecular calculations and DFT

Nearly all molecular calculations have the goal to solve the Schroedinger equation, Equation 1.7 [5]:

$$\hat{H}\psi_i = E_i\psi_i \tag{1.7}$$

Stationary Schroedinger equation. $\hat{H}$ represents the Hamilton operator. ψ is the Wave function of the system and E is its energy.

More information is needed, if this eigenvalue problem has to be solved. The Hamilton operator of a many-body-problem consists of five different parts as seen in Equation 1.8.

$$\hat{H} = \hat{V}_{cc} + \hat{V}_{ec} + \hat{V}_{ee} + \hat{T}_{ke} + \hat{T}_{kc} \tag{1.8}$$

Separation of the Hamilton operator. $\hat{V}_{cc}$ describes the interaction of the cores to each other. $\hat{V}_{ce}$ stands for the interaction of core and electron. $\hat{V}_{ee}$ is the electron-electron interaction and the $\hat{T}_{ke}$ and $\hat{T}_{kc}$ terms represent the kinetic energy of electrons and cores.

This combination of numerous variables makes the Schroedinger equation for most cases not exact-solvable. Approximations are needed to get any results.

One possible simplification is the Born-Oppenheimer-approximation.
Nucleons have a much higher mass then electrons, about 1800 times higher. This means that electrons may move much faster then the core particles. This allows electrons, formally, to move free while the cores are stationary. In this case the electron-movement can be calculated for each core position separately.
Most systems will have more than one electron and therefore the electron calculation itself is still a many-body-problem. To get rid of this numerical solution paths were created and the most common is nowadays Density Functional Theory.

1.3 Density Functional Theory

DFT is based on the two Hohenberg-Kohn theorems, named after Walter Kohn and Pierre Hohenberg.

The first theorem connects the energy of the electronic ground state in a system, E, directly to an unknown functional, $F[\rho(\vec{r})]$, of the electron density $\rho(\vec{r})$.
The electron density describes the possibility of an electron to appear on a certain position, it is a function of the distance $\vec{r}$. Integration over the whole electron density must result in the total amount of electrons in the system.

The second theorem declares that the principle of variation is also valid for the electron density because all electron densities result in higher electronic ground state energies than the exact solution of the system, Equation 1.9.

$$F[\rho(\vec{r})] \geq E_{exact} \tag{1.9}$$

Principle of variation. $F[\rho(\vec{r})]$ is the electronic ground state functional depending on the electron density ρ which itself depends on the radius $\vec{r}$. E_{exact} is the electronic ground state energy

This also means that it is possible to calculate the energy when an electron density is given, even if the wave function is not known, which is an advantage in comparison to Hartree Fock or Configuration Interaction.
Approximations have to be done, since the exact functional is unknown. The problem of the functional calculation is divided into the sum of three functionals, similar to the Hamilton operator separation, Equation 1.10 [6].

$$F[\rho] = T_e[\rho] + E_{ec}[\rho] + E_{ee}[\rho] \tag{1.10}$$

Separation of the functional in DFT. The first functional describes the kinetic energy of the electrons $T_e[\rho]$. The second represents the interaction between cores and electrons $E_{ec}[\rho]$. The last part of the original functional is the interaction of electrons with each other $E_{ee}[\rho]$.

Some problems remain even with simplifications like the Born-Oppenheimer approximation. One is the calculation of the kinetic and the exchange energy. This problem was approached by Walter Kohn and Lu Jue Sham which resulted in the Kohn-Sham-DFT (KS-DFT). In these DFT calculations all electrons are separated into one electron wave functions.

The Hamilton operator was manipulated and represented via two energy terms. One term is a constant term and the other one is dependent of a parameter λ. The constant term is the exact Hamilton operator and the dependent part is the electron-electron interaction Equation 1.11.

$$\hat{H}_\lambda = \hat{T} + V_{ext} + \lambda V_{ee} \tag{1.11}$$

KS-DFT Hamilton representation. V_{ext} is a external potential in which the electrons are moving.

The electron density must be constant for all λ. If λ is zero no electron-electron interaction exists which means that the system includes only one electron and an exact solution is obtained. In most cases λ will not be zero and therefore the exact solution is, due to the unknown exchange correlation functional, not obtainable. For this case again only approximations can be made. Those are defined via the used functional (local density approximation (LDA), Perdew-Burke-Ernzerhorf (PBE), Becke three-parameter Lee-Yang-Parr (B3LYP), etc.) [6].

1.4 VASP and plane-wave DFT

VASP is a computer program designed for ab initio calculations of electronic structures .
This program uses plane wave basis sets [7, 8, 9], the equation for a plane wave is given in Equation 1.12.

$$\psi(r) = \frac{1}{\Omega} * e^{i*(G+K)*r} \tag{1.12}$$

$\psi(r)$ is the plane wave itself. Ω is the volume of the unit cell G is the reciprocal lattice and brillouin zone and k its projection .

This concept of basis set is important for the introduction of the energy cut off, the used value will be mentioned in chapter 2. The Energy cut off is defined by Equation 1.13.

$$E_{cut\ off} \geq \frac{1}{2}|G+K|^2 \tag{1.13}$$

Energy cut off for plane wave basis set.

The energy cut off can be equal or greater than the highest kinetic energy of the used plane waves. A smaller energy cut off may result in wrap around errors[10].

In this thesis we will only use the Kohn-Sham-DFT-GGA method in VASP. GGA stands for Generalized Gradient Approximation, which means that not only the density itself is used for the calculation but also the first differential of the density in respect to the location. This should result in higher efficiency.
In this thesis, we employed PBE as correlation-functional. PBE has no semi empirical background but it is an ab initio (first principles) functional [11]. Another functional for such calculations would be PBE0 which combines PBE exchange energy, PBE correlation energy and Hartree-Fock exchange energy to its exchange

correlation energy and is therefore a hybrid functional. The used potentials are created from projected-augmented wave method [12, 13], obtained from the VASP library.

These potentials are needed for a better description of the valence electrons and are known to be more accurate than most of the available pseudo potentials [13]. A successful calculation in VASP will result in two different criteria for total convergence, one criteria concerns the structure and one the energy. VASP will always calculate an ion displacement loop in which will be the energy convergence loops.

1.4.1 Nudge elastic band method (NEB)

The NEB describes an additional script implementable in VASP which allows to take care of transition state calculations.

This will be needed for calculations of systems during the movement of ions from one position in the lattice to another previously empty position in the lattice.

NEB calculations need in comparison to normal VASP calculations additional input parameters as seen in section 2.2, as well as sub-directories. Within each sub-directories is one POSCAR file describing the system which shall be calculated.

Classic DFT calculations would converge to a state with low energy but in this case higher energies are desired. Therefore the climbing image NEB (CI-NEB) method, from University of Texas, moves the atoms upwards in energy towards the saddle point with unequal distances between the images. This creates a system that converges at saddle point, which is preferable for ion movement, and the unequally distanced images create a faster convergence than equally distanced points from NEB alone [14, 15]. The obtained saddle point of the moved ions is equal to the energy barrier in ion movement and can be compared to experimental data. Typically obtained data in form of a diagram representing the different calculation

points of NEB is given in Figure 1.5 .

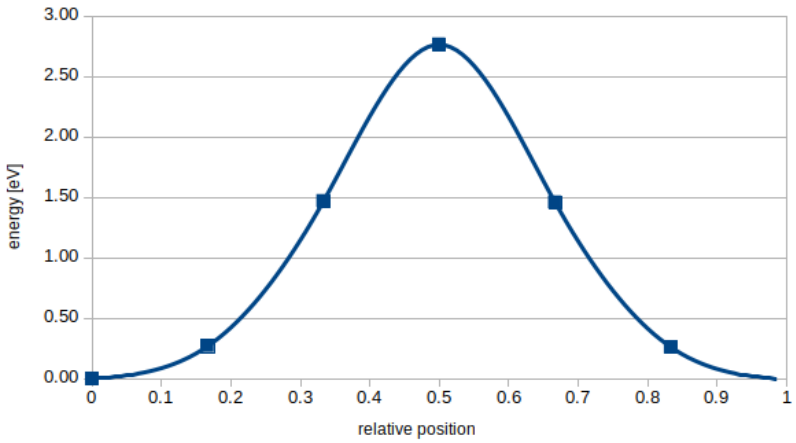

Figure 1.5: Example for NEB results. F^- ion energy barrier profile in $BaLiF_3$ the x axis represents the relative position of the moved ion on the NEB path. The y axis is the energy of the system. Every point represents a calculated position. The maximum of the Energy is the energy barrier the ion has to overcome if it travels along this path.

1.4.2 Simulation of higher temperature

In basic VASP calculations, which were described so far, only calculations at 0 K are done, but energy-barriers at higher temperature are needed to be comparable to experimental results.

Temperature is simulated by vibration, in terms of the harmonic oscillator approximation, of atoms in the system. To introduce those vibrations a combination of the program Phonopy with VASP will be needed for the unit cell. These calculations are time consuming, therefore it is useful to calculate only the starting and the transition state position with the highest energy obtained by CI-NEB. For repeating units of higher order, the IBRION = 5 tag can and will be used, section 2.2.

In harmonic oscillators, the zero point energy E_{ZP} is given by the sum over the

obtained vibration-mode frequencies, Equation 1.14:

$$E_{ZP} = \sum_{n=1}^{3N-3} \frac{1}{2} * h * \nu_n \tag{1.14}$$

Zero point energy. N is the number of atoms in the system. h is the Planck's constant and ν is the frequency of the vibration.

This term itself is not sufficient for our calculations but it can be used to correct the earlier obtained energy from the non vibrating system, Equation 1.15:

$$H_0 = E + E_{ZP} \tag{1.15}$$

H_0 is the enthalpy and represents a corrected version of the energy in the system.

A propabillity for each state to be occupied can be introduced by using Boltzmann distribution,Equation 1.16:

$$p_i = e^{\frac{-E_i}{k_b * T}} \tag{1.16}$$

k_b is Boltzmanns constant. E_i is the energy of the harmonic state i. T is the temperature.

The enthalpy for N different particles is given in Equation 1.17 [16]:

$$H = k_b T^2 (\frac{\delta ln(p_i^N)}{\delta T})_V + k_b T V (\frac{\delta ln(p_i^N)}{\delta V})_T \tag{1.17}$$

V is the volume of the system

A similar relation is known for the entropy given in Equation 1.18 [16]:

$$S = k_b T (\frac{\delta ln(p_i^N)}{\delta T})_V + k_b ln(p_i^N) \tag{1.18}$$

The zero point energy depends strongly on higher frequencies since frequencies are summed up, but dS and dH depend on lower frequencies, because those have lower energies. Those lower frequencies are more challenging to describe and introduce larger errors than the zero point energy.
Both, entropy and enthalpy are most of the time represented as their difference to the zero point value. Those differences are dS and dH respectively.
The energy barrier in the system is the difference between to states, section 1.2. If the system is not at 0K but at higher temperatures the Gibbs free energy is needed, Equation 1.19:

$$dG = dH - TdS = E_{barrier} \tag{1.19}$$

dG is the difference in Gibbs free energy and dS is the difference in entropy.

We are going to use the Gibbs free energy as a compare able energy barrier with the experiment since impedance spectroscopy is not done at 0 K. Higher temperatures are as mentioned not necessarily lowering the calculated energy barrier [4], in some cases a small increase will be noticed.

1.5 Barium Lithium Fluoride

The structure of $BaLiF_3$ was determined with x-ray analysis. The result is shown in Figure 1.6. $BaLiF_3$ represents an inverse perovskite in a cubic crystal and a space group of PM-3m [17, 18, 19].

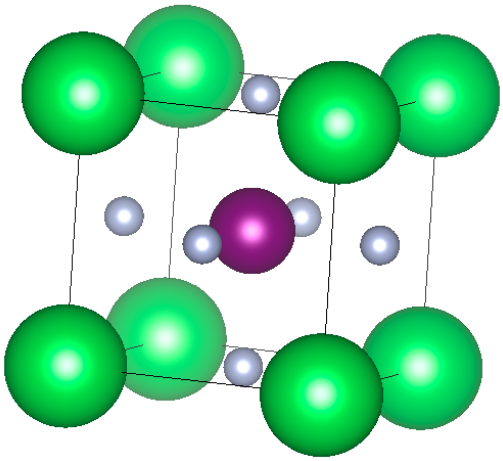

Figure 1.6: $BaLiF_3$ unit cell
green = Barium, violet = Lithium, grey = Fluor

It can be seen in Figure 1.6 that all F are relative to Ba and Li in the same position. This circumstance allows to only calculate the energy barrier for one moving F^-- ion representing all F^-.

It is trivial that Ba and Li calculations in this cell size are pointless since there is only one atom of those elements in the unit cell. It may seem in Figure 1.6 as if there are 8 Ba-atoms in the unit cell, but each of those 8 Ba-atoms contributes only to $\frac{1}{8}$ inside of the unit cell. In larger cells it becomes obvious that F^- has more possible paths, this will be shown and discussed in section 4.1. Larger cells also allow Li to move between positions of its sub lattice.

In the unit cell the additional calculation for the exchange of Ba^{2+} with Li^+ is done by simply changing the position of Li^+ with Ba^{2+} and calculate the F^- and

Li^+ movement with all additional paths again. The Li-Ba-exchanged structure for a 2x2x2 cell is shown in Figure 1.7.

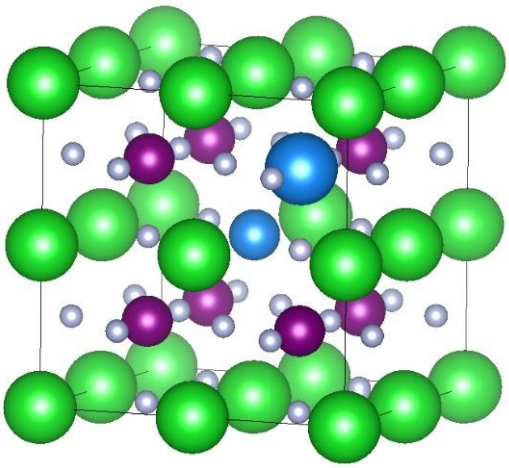

Figure 1.7: $BaLiF_3$ 2x2x2 cell with exchanged Ba and Li
green = Barium, violet = Lithium, grey = Fluor, exchanged Ba and Li are blue

In bigger repeating units the amount of exchanged Li^+ and Ba^{2+} may also influence the energy barrier for the ion movement and therefore all ion movements must be calculated in super cells of different atom exchange concentrations. Additionally to the already known paths in the unexchanged structure opens the exchange of Lithium with Barium now the possibility of Li^+ at the Ba^{2+} position to move to a Li^+ position and to move to an empty Ba^{2+} position, those paths will be shown in section 4.2.

Calculations

2.1 Fluor gas, bcc-bulk-Lithium

To calculate the defect formation energy, as shown in section 1.2, the energy of the formed additional materials is needed. This energy will be gained in the vacancy formation and therefore changes the defect formation energy, shown in Equation 1.3.

In this thesis,F^-defects are created which result in the formation of half a F_2-molecule. The energy for F_2 can be calculated also via VASP with the same conditions as $BaLiF_3$ unit cell optimization.

One other created defect is the Li^+ point defect. Since Li^+ does not form molecules with itself a body-centred-cubic (bcc) structure for bulk Li was used for energy calculations, also with the same conditions as for $BaLiF_3$ unit cell.

Li^+ may also change from a Ba^{2+} position to an empty Ba^{2+} position as discussed in section 1.5, therefore the defect formation energy of Ba^{2+} point defects has to be calculated. A bcc Ba was used for bulk calculations.

2.2 Input

$BaLiF_3$ consists of Barium Lithium and Fluor. These elements need to be considered for the calculation with VASP. The used PAW-potentials implemented in the VASP program are Ba_ sv, F and Li. The sv therm in Ba_ sv indicates that s and p electrons are also treated as valence electrons [13].

The maximal energy in these potentials is 400 eV and therefore our limit for the calculation is 600 eV which is even higher than the proposed cut off for each element (Ba_ sv cut off = 187 eV, F cut off = 400 eV, Li cut off = 140 [20]). This is needed to correct possible resulting Pulay stress from cell deformation during cell optimization [21]. This value is given in ENCUT in the INCAR file.
For the ion movement it is essential to identify which ions are of interest. In this work we will take a closer look to the Li^+ and the F^- ion movement in $BaLiF_3$ with respect to the possibility of Li^+ changing place with Ba^{2+}.

The first step in the following calculation for ion movement is the optimization of the structure obtained by x-ray analysis. Afterwards the defect structures for different defect concentrations and different ions can be optimized. The third step will be the CI-NEB calculations for all ions and defect concentrations. Followed by the introduction of vibration in the transition and ground states via Phonopy or changed VASP-tags.

2.2.1 VASP input overview

There are four input files needed to start calculations in VASP. One is the POSCAR file which includes the structure of the system. The POTCAR file includes the used PAWs. KPOINTS defines the dimensions of the calculation and INCAR has a large variety of parameters and settings for the calculation. In this section

some important parameters from INCAR for the following calculations will be discussed. Input parameters may change between calculation types. Parameters given in Table 2.1 are for structure optimization.

Table 2.1: INCAR parameters for structure optimization and NEB [22]

Parameter	Value	Description
GGA	PE	is a GGA-Type functional PE defines it as PBE-Functional.
EDIFF	1E-5	is the energy convergence criteria.
ENCUT	600	is the energy cut-off related to the plane waves as described in section 1.2.
LREAL	.TRUE. or Auto	.TRUE. will be used for the unit cell since it is quite small in our case. Bigger cells, like the 2x2x2 cells, should already be calculated with Auto.
IBRION	1	Ions are relaxed. IBRION 5 includes vibrational frequencies in the calculation.
ISIF	3	defines which parameters may change for the calculation. With ISIF = 3 the ions are relaxed and the cell volume as well as its shape may change. For ISIF = 0 for example only the ion are relaxed but the cell stays the same.
additional NEB parameters		
IMAGES	2	makes NEB calculations with 2 intermediate structures.
SPRING	-5	keeps the images in equivalent distance via tangential springs.
LCLIMB	.TRUE.	enables climbing image NEB, in this case SPRING is not needed.

2.3 Movement in Super Cells

Optimization of the unit cell is done by using the input ISIF = 3, since the volume of the cell and the positions of the atoms shall not be fixed. Following transition state calculations and defect creation will be done with ISIF = 0, the change of the cell size is not wanted if a defect occurs.
Unfortunately, the defect concentration in $BaLiF_3$ is unknown and a variety of concentration must be tested. With the decrease of unit cells in the super cell the varieties of possible defects and defect concentrations increase drastically. Therefore only a few examples will be presented here. An overview of calculated defect concentrations in this work is given in Table 2.2.

Table 2.2: defect concentrations

cell dimensions	K-points	number of defects in cell	defect concentration in super cell
1x 1x 1 unit cell	5 5 5	1	0.200
1x 1x 1 unit cell	3 3 3	2	0.400
2x 2x 2	3 3 3	1	0.0250
2x 2x 2	3 3 3	2	0.050
2x 2x 2	3 3 3	3	0.075
3x 3x 3	2 2 2	1	0.007
3x 3x 3	2 2 2	2	0.015
3x 3x 3	2 2 2	3	0.022

The mentioned K-points in the previouse table give the size of the reciprocal space cell. The total cell size should be approximately 20 Å and the $BaLiF_3$ unit

cell (1x 1x 1 cell) has a lattice parameter of 4 Å .Therefore, with a 1x 1x 1 cell we need 5 K-points and less K-points if the real space cell size increases. Introducing of a defect in the unit cell can be done by taking out one of the F^-- ions. The combination of defect-less results, F_2 building energy and defect-results allows us to calculate the defect formation energy, as shown in Equation 1.3.

The created vacancy can then be used to calculate the movement of one remaining F^-- ion from its previous position to the position of the vacancy.
If a very high defect concentration is assumed, a unit cell with two F^- vacancies and one moving F^-- ion can be introduced. It is easy to understand that for the unit cell the Li^+ movement calculation is pointless since a remove of the Li^+ ion would create a material completely without Li, but in bigger super cells the calculation works the same way as with F^-.
The exchange of one Li^+ with one Ba^{2+} in the super cell must also be considered for the F^- and the Li^+ ion movement, this increases the number of calculations.
For the unit cell a system of 5x5x5 K-points was created to gain a calculation size around 20 angstroms in each dimension, since the optimized unit cell has a lattice parameter of 4.01 Å . When the size of the super cell increases the K points have to shrink to stay in the preferred calculation volume.
In this work super cells of symmetrical size in all three dimensions were used, but other super cells are possible as well.

2.4 Dispersion

In this work a dispersion correction will be used to describe van der Waals interaction between temporarily induced dipoles. The energy correction is shown in Equation 2.1.

$$E = E_{KS-DFT} + E_{disp} \tag{2.1}$$

E is the corrected energy term.E_{KS-DFT} is the energy obtained from Kohn Sham DFT calculation and E_{disp} is the dispersion correction term.

The method used to calculate E_{disp} is given in the INCAR file by setting the IVDW tag. In cell optimizations IVDW = 12 will be used, this indicates the use of DFT-D3 method with Becke-Jonson damping [23, 24]. DFT-D3 uses the energy dispersion given in Equation 2.2.

$$E_{disp} = -\frac{1}{2}\sum_{i=1}^{N_{at}}\sum_{j=1}^{N_{at}}\sum_{L} f_{d,6}(r_{ij},L)\frac{C_{6ij}}{r_{ij,L}^{6}} + f_{d,8}(r_{ij},L)\frac{C_{8ij}}{r_{ij,L}^{8}} \tag{2.2}$$

with N_{at} as the number of atoms. r as the relative position from atom i to atom j. L is the translation of the unit cell. C_{6ij} and C_{8ij} as dispersion coefficients and $f_{d,6}$ the Becke-Jonson damping given in Equation 2.3.

$$f_{d,n}(r_{ij}) = \frac{s_n}{1+6(r_{ij}/(s_{R,n}R_{oij}))^{-\alpha_n}} \tag{2.3}$$

$R_{0ij} = \sqrt{\frac{C_{8ij}}{C_{6ij}}}$. α_6 is 14 α_8 is 16 and $s_{R,8}$ is 1. the other parameters are adjustable and can be given in the INCAR file, the used values for this calculation are given in the example INCAR in the appendix, section 4.4.

The mentioned tag IVDW with value 12 is only used for optimization since NEB calculations need a older VASP version which does not include IVDW = 12, instead LVDW = .TRUE. will be used. This will not include the mentioned DFT-D3 method but DFT-D2. DFT-D2 is a more simplified approach to dispersion correction with the energy term given in Equation 2.4 [25].

$$E_{disp-D2} = -\frac{1}{2}\sum_{i=1}^{N_{at}}\sum_{j=1}^{N_{at}}\sum_{L} f_{d,6,d2}(r_{ij},L)\frac{C_{6ij}}{r_{ij,L}^{6}} \tag{2.4}$$

$E_{disp-D2}$ is the dispersion correction energy with the DFT-D2 method. $f_{d,6,d2}$ is the DFT-D2 dumping given in Equation 2.5

$$f_{d,6,d2}(r_{ij}) = \frac{s_6}{1 + e^{d(r_{ij}/(s_R R_{0ij})-1)}} \tag{2.5}$$

e is Euler‘s number. All other parameters are the same is for the dumping in DFT-D3.

This dispersion will be used by VASP to calculate the free energy at the very last step of each ion-loop. This can be seen by the sudden upwards jump of the free energy at each last step, no such jump will occur if dispersion correction is not used.

Experiment

To obtain the energy barrier out of experiment, the relation of energy barrier and conductivity, Equation 3.1 is needed.

$$\sigma * T = \sigma_0 * e^{\frac{-E_{barrier}}{k*T}} \tag{3.1}$$

Relation between conductivity and the energy barrier. σ is the conductivity.

The conductivity can be obtained with impedance spectroscopy [26].
In impedance spectroscopy, the conductivity is measured as a function of frequency for constant temperature [27]. The experiment itself is done by applying an alternating voltage and measuring the obtained current with its corresponding time delay which is, since the current and the potential are of sinusoidal form, the phase shift as seen in Figure 3.1.

Figure 3.1: phase shift

Voltage over time in pink and current over time in blue. The phase shift can be seen by the different time the maxima appear, without phase shift those maximums would occur at the same time.

For further investigation the impedance is introduced, representing the resistance in the complex plane.

$$Z(\omega,t) = \frac{U(t)}{I(t)} = \frac{U_m * sin(\omega * t)}{I_m * sin(\omega * t + \theta)} = \frac{sin(\omega * t)}{sin(\omega * t + \theta)} * |Z| \tag{3.2}$$

Z is the impedance. U is the applied potential. I is the observed current. ω is the circular frequency. t is the time and θ is the phase shift between current and potential.

Admittance Y is given by the reciprocal of the impedance.

With known area of the sample A as well as its thickness d Equation 3.3 can be used to obtain the specific admittance.

$$\sigma_Y = Y * \frac{d}{A} \tag{3.3}$$

The specific admittance σ_Y in relation to the admittance Y and the area A as well as the thickness d of the sample.

The so obtained specific admittance can be separated into a real and an imaginary part, Equation 3.4.

$$\sigma_Y = \sigma_r + i * \sigma_i \tag{3.4}$$

Separation of specific admittance into real σ_r and imaginary σ_i part.

With these relations, it is possible to plot the real part of the specific admittance against frequency ν [28]. This will result in a graph with a slope close to zero for high temperatures in the low frequency regime. The σ of this plateaus is called σ_{DC} and can be used to obtain a $ln(\sigma_{DC} * T)$ versus $\frac{1}{T}$ plot following Equation 3.5 which resulted from introducing σ_{DC} into Equation 3.1. Therefore, a straight line is gained with $\frac{-E_{barrier}}{k}$ as its slope. The slope divided by the Boltzmann constant results in the energy barrier itself.

$$\sigma_{DC} * T \sim e^{\frac{-E_{barrier}}{k*T}} \tag{3.5}$$

$$ln(\sigma_{DC} * T) \sim \frac{-E_{barrier}}{k} * \frac{1}{T} \tag{3.6}$$

Relation of σ_{DC} to $\frac{1}{T}$

The so evaluated experimental energy barrier should match with the calculated energy barrier from the CI-NEB calculations.

Results

The optimization of the $BaLiF_3$ unit cell resulted in a cell with a lattice constant of 4.01 Å which is compared to 3.99 Å obtained by x-ray diffraction [29] and 4.04 Å obtained by previous DFT calculations [30]. The difference between x-ray value and our DFT calculation may exist because of the temperature difference, but also due to the fact that GGA-functional was used which tend to overestimate the lattice constant. To see if GGA resulted in the higher lattice constant one optimization with LDA, which normally underestimate lattice parameters [31], was done, the results are shown in Table 4.1. As expected LDA resulted in a lower lattice constant then GGA and was also further away from the x-ray diffraction result.

Table 4.1: lattice parameter

x-ray diffraction	GGA	LDA
3.99 A	4.01 A	3.89

4.1 Fluor conductivity

The calculated formation energy of F_2 is -3.56 eV.

The defect formation energy of the Fluor defect was found to be in average 5.93 eV. If the value is true, there would not be a single defect in one mol material, at appropriate temperatures and the probability of having ion conductivity with presented mechanism would be close to zero. Similar defect formation energies were found by molecular dynamics simulation of $BaLiF_3$ [32]. In previous work and other materials, lower defect formation energies could be found for defects close to other defects [33]. This phenomenon could not be observed in this case meaning the defect formation of F or Li close to the exchange of Ba^{2+} with Li^{+} (second defect) was not drastically lower than the defect formation energy without exchange of B^{2+} and Li^{+}. The defect formation energy for F-defect in the exchanged structure was found to be 6.48 eV , which is even higher than for the non exchanged structure. The defect building energy of the exchanged structure itself was found to be 7.65 eV. This value is also higher than expected especially since previous work shows an energy difference of 1 eV [32].

There are two possible paths for F^{-}-conduction, one is in-between two Ba parallel to one side of the unit cell and the other one is through the unit cell in-between a Li and a Ba, those paths are shown in Figure 4.1 showing a 2x2x2 cell.

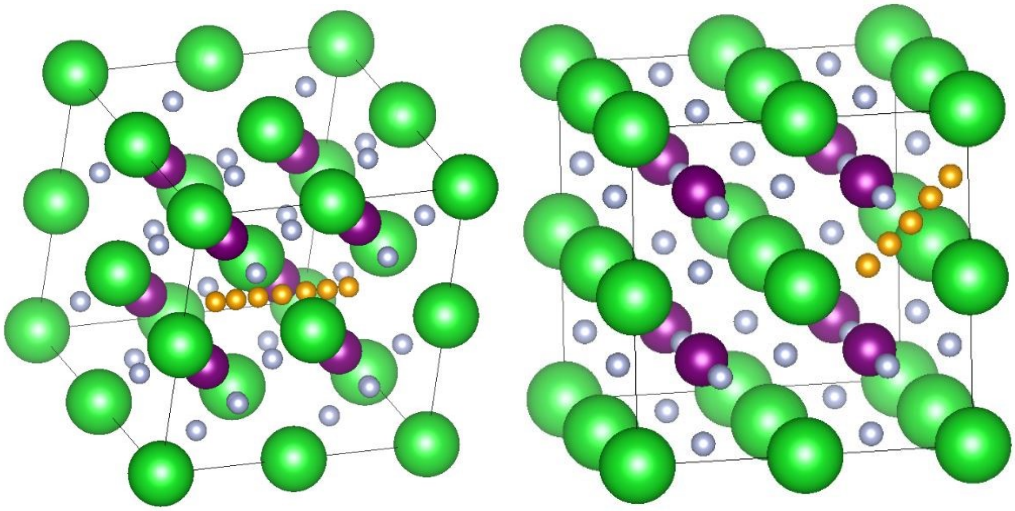

Figure 4.1: F^- ion paths in $BaLiF_3$
left: Fluoride path between two Barium, right: Fluoride path between Lithium and Barium

The energy barrier for the F^- paths are given in Table 4.3 and the energy profiles for both F path is given in Figure 4.2.

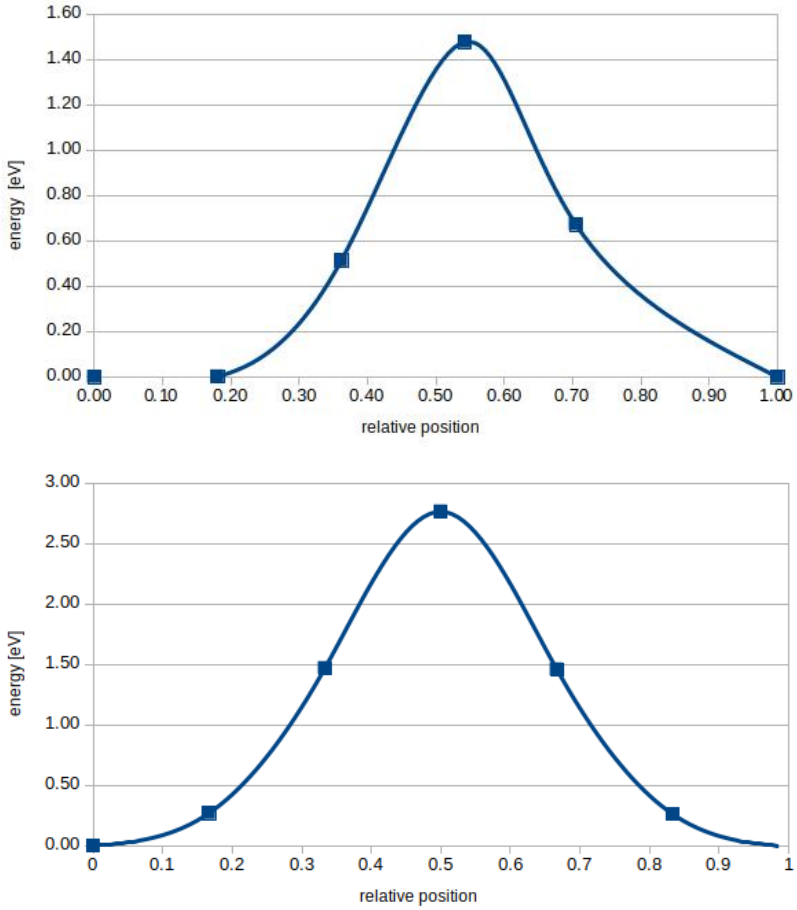

Figure 4.2: F^- ion energy barrier profile in $BaLiF_3$

The upper profile was obtained by F movement in the unit cell (F moving in between Li and Ba). The lower profile represents F-movement between two Ba^{2+} in a 2x2x2 super cell. The relative position indicated by the x axis shows 0 and 1 as already optimized structures.The calculation points in between are from CI-NEB.

It can be seen that the start and end point are energetically equivalent since these positions are symmetrical to each other. There exists only one maximum. The effect of using CI-NEB can be seen in the different spacing in between the images.

Table 4.2: average F-energy barrier

cell	**K-points**	**F between two Ba [eV]**	**between Li and Ba [eV]**
1x 1x 1	5 5 5	-	1.48
2x 2x 2	3 3 3	2.62	0.81
3x 3x 3	2 2 2	2.65	1.14

The calculation of F^- movement in $BaLiF_3$ unit cell as well as repeating unit of 2 unit cells and 3 unit cells indicates that the energy barrier is dependent on the size of the repeating unit and therefore the defect concentration. If the repeating unit increases in size the energy barrier decreases. Small repeating units include that the defect concentration is high and the ion movement is done often close to each other therefore hindering each other, in bigger repeating units this effect will not be so strong, resulting in convergent energy barrier with increasing cell size.

The Results of the Zero point energy (ZPE) correction obtained from vibrational calculations are shown in section 1.4 and the calculation of Gibbs free Energy (dG) are given in Table 4.3.

Table 4.3: average F-energy barrier with ZPE and temperature correction

path	**cell**	**K-points**	**defects**	**dE [eV]**	**dH=dE+ZPE [eV]**	**dG=dH-TdS at 300 K [eV]**
Fli	1x 1x 1	5 5 5	1	1.48	1.77	1.76
	2x 2x 2	3 3 3	1	0.51	0.54	0.63
			2	0.97	1.01	1.02
			3	0.96	0.98	0.99
Fba	2x 2x 2	3 3 3	1	2.77	2.79	2.83
			2	2.77	2.79	2.97
			3	2.32	2.34	2.58

Fli is the F-path in between Li and Ba, Fba is the F-path in between two Ba. defects represents the number of defects in the cell.

The exchange of Lithium with Barium in the unit cell did change the energy barrier for both F^- paths. The defect concentration and cell size were also influencing the energy barrier for the exchanged structure. The obtained average energy barriers for F-transition in the exchanged structure is 1.08 eV between two barium and 0.41 eV between a lithium and a barium. The energy barrier in the exchanged structure is lower to the one obtained in the unexchanged structure.

Experimental data obtained from impedance measurements indicate an energy barrier for on conduction in $BaLiF_3$ of approximately 0.76 eV [34, 35, 36] and are therefore in relatively good agreement to our calculated values between 0.63 to 1.02 eV for the unexchanged structure. The upper limit of 1.76 is not really trustworthy since it was calculated in the small unit cell which always gives high energy barriers. But the defect formation energy for the exchanged structure and the additional F point defects is quite high and therefore F-movement in the unex-

changed structure in between Li and Ba should be favoured.

The so far used PBE functional is of course not the only possible functional for this type of calculations, another functional would be PBE0. PBE0-D3 functional was used to make some single point calculations. Single point calculations implies, that there is no ion but only electron relaxation. The used PBE0-D3 functional is a semi empirical hybride functional and should result in more accurate results, but the calculation time is also increased, which made it not the choice from the beginning. The obtained energy barriers for single point PBE0-D3 analysis of all F-paths in the unexchanged structure is given in Table 4.4

Table 4.4: single point F-energy barrier

path	**cell**	**K-points**	**defects**	**dE [eV]**
Fli	1x 1x 1	5 5 5	1	0.99
	2x 2x 2	3 3 3	1	0.48
Fba	2x 2x 2x	3 3 3	1	2.63

The energy barrier from the 1x1x1 cell , the unit cell, now fits well in our over all interval for Fli-energy barrier since it is significantly lower than from the PBE calculations. Nearly no change is observable for the 2x2x2 cell.

4.2 Lithium conductivity

The bcc-Li-bulk calculation resulted in an energy of -2.06 eV per Li atom and Ba-bulk calculations results in -2.12 eV per atom.

Average defect formation energy for Li-defects of 6.41 eV for the unexchanged structure could be obtained.
It was seen that for Li^+ the defect formation energy in the non exchanged structure is too high to result in ion conduction, and only the exchanged cells results in reasonable defect formation energies of 1.01 eV for the defect formation of Li-defect on a Ba lattice position. The defect formation energy of Li on a lithium position in the exchanged structure is 7.25 eV, which is also higher compared to the unexchanged structure. Ba defect formation energy was extremely high with 12.24 eV.
One possible path for the Li^+-ion movement in the unexchanged structure was found. The path is shown in Figure 4.3 and the corresponding energy is given in Table 4.5.

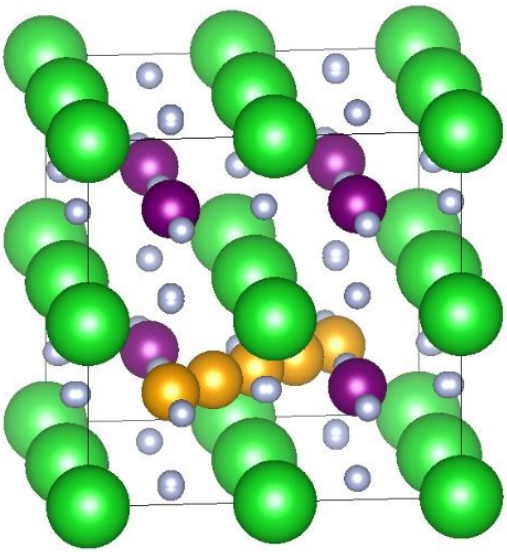

Figure 4.3: only Lithium path in $BaLiF_3$

Table 4.5: Li-energy barrier

cell	**K-points**	**defects**	**Li-path energy barrier dE [eV]**	**dH = dE +ZPE [eV]**	**dG = dH -TdS [eV]**
2x 2x 2	3 3 3	1	3.88	3.90	3.82
		2	3.84	3.68	3.63
		3	3.60	3.60	3.41

These values are still quite high and would result in low conductivity at reasonable temperature. Bigger super cells of 3x3x3, which means lower defect concentration, resulted in a somewhat lower energy barrier (dE) of 3.49 eV. The energy profile is given in Figure 4.4.

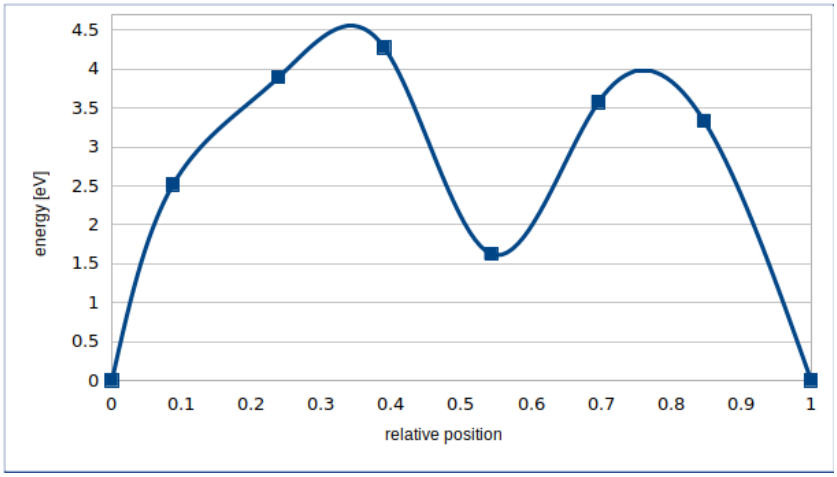

Figure 4.4: Li^+ energy profile in the non-exchanged structure of $BaLiF_3$.

The curve is more or less symmetrically since the start and end point are symmetrical to each other. Two maxima can be seen in the shown Li-path. Those maxima represent the two positions in the path were the Li has to pass in between two F of a unit cell. This can also be seen in the relative position, we would expect a maximum at 0.25 and 0.75 and this is the case. Small differences in the position of the maxima result from the relaxation of the F particles.

In the Ba^{2+} and Li^+ exchanged structure two additional Li^+ paths are possible, both paths are shown in Figure 4.5 and the calculated energies are given in Table 4.6.

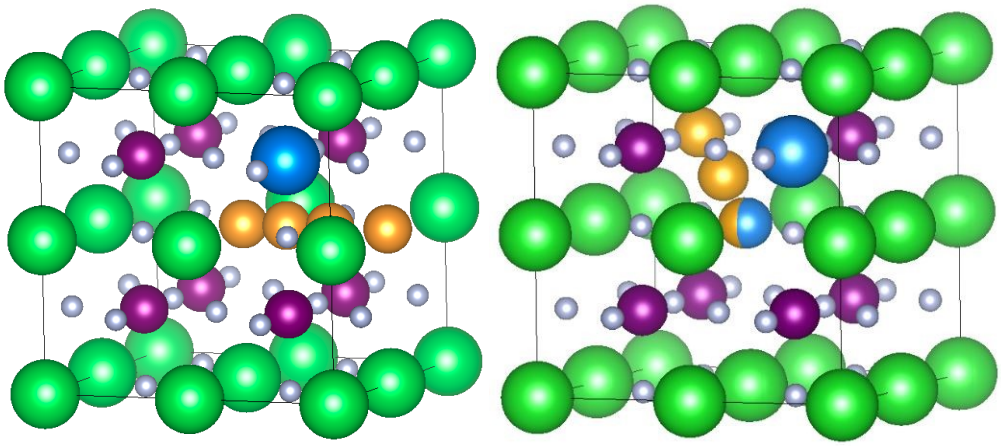

Figure 4.5: Li^+ ions in exchanged $BaLiF_3$
left: Lithium path on Barium sub lattice, right: Lithium path from Barium to Lithium sub lattice

Table 4.6: average Li-energy barrier exchanged structure

cell	**K-points**	**Li-path from Ba sub lattice to Ba sub lattice [eV]**	**Li-path from Ba sub lattice to Li sub lattice [eV]**
2x 2x 2	3 3 3	2.20	7.55

Since impedance spectroscopy can not indicate which ion is responsible for the obtained data the same values have to be taken for F^- and Li^+ conduction. The calculated energy barriers for Li^+ in $BaLiF_3$ are most of the time much higher as the experimental values mentioned in section 4.1. Except for the Li-path in the exchanged structure between two Barium sub lattice positions, but this path has an extra ordinary high defect formation energy. This result of higher energy barrier for Li^+ conduction is not surprising since a good match of F-conduction and experiment was obtained, if Li-conduction would have an even lower energy barrier the experiment would only show the Li-conduction.

The only found Li^+ path in the unexchanged structure was analysed by single

point calculation with the PBE0-D3 functional. The so obtained energy barrier was 3.87 eV. This value is a little bit higher than the obtained energy barrier from the PBE functional calculations.

Summary

The results from this thesis indicate that the experimentally obtained values for ion diffusion in $BaLiF_3$ are from F^- ions moving between a barium and a lithium in the unexchanged structure. Other obtained paths had significantly higher energy barriers. One calculated path resulted in an somewhat lower energy barrier than the experiment, but this path was in the exchanged structure which has a high defect formation energy itself.
Li^+ in the exchanged structure at the previous Barium position was the only defect with a reasonable low defect formation energy. The high defect formation energy was also found in previous calculations on this material [18] and this may indicate that some additional impurities are needed for defect formation. A proposed strong influence of Ba-Li-exchange defect on the activation energy could not be seen for Schottky defects in this work although previous calculations for Frenkel defects in this material resulted in lower activation energies [32]. The values for the energy barrier are not perfectly converged in respect to the cell size, bigger cells would probably result in slightly lower energies but this should not influence the underlying principles and relation of the different paths to each other significantly.

Future investigation on this material should include more calculations with hybrid functionals like PBE0-D3, since those could lower the energy barrier as seen in

section 4.1 and should include additional paths in the exchanged structure. In this work, only a single Li^{+} was exchanged with Ba^{2+} but more than one exchange could be possible and thus lead to additional paths, for example F^{-} in between two exchanged Li^{+} etc.

Appendix

4.3 Used Programs

VASP.5.4.1. for calculations without climbing image NEB

VASP.4.2 for calculations with climbing image NEB

Phonopy for the frequency calculation of the transition state in the unit cell

VESTA for visualizing

4.4 Example files

POSCAR of $BaLiF_3$ unit cell obtained by x-ray diffraction

```
ba1 f3 li1
   1.00000000000000
     3.9920001030000001    0.0000000000000000    0.0000000000000000
     0.0000000000000000    3.9920001030000001    0.0000000000000000
     0.0000000000000000    0.0000000000000000    3.9920001030000001
   Ba   Li   F
     1     1     3
Direct
  0.0000000000000000  0.0000000000000000  0.0000000000000000
  0.5000000000000000  0.5000000000000000  0.5000000000000000
  0.5000000000000000  0.5000000000000000  0.0000000000000000
  0.0000000000000000  0.5000000000000000  0.5000000000000000
  0.5000000000000000  0.0000000000000000  0.5000000000000000
```

KPOINTS of 2x2x2 cell of $BaLiF_3$, repeated three times in every dimension

```
Auto
0
Gamma
 3  3  3
 0  0  0
```

INCAR example for $BaLiF_3$

```
SYSTEM = BaLiF3

Electronic minimisation
GGA = PE
PREC = Accu
EDIFF = 1E-5
EDIFFG = -0.005
ENCUT = 600
NELMIN = 4
NELM = 400

ISPIN = 2
LREAL = .FALSE.

NPAR=4

 DOS related values
 SIGMA  =    0.01
 ISMEAR =    0

! Ionic relaxation
  NSW    =     300
 IBRION =      1
 ISIF = 0

  LORBIT= 12

LVWD = .TRUE.
VDW_VERSION = 4
VDW_RADIUS = 50.0
VDW_CNRADIUS=15.0

VDW_s6 = 1.0
VDW_s8 = 0.7875
VDW_a1 = 0.4289
VDW_a2 = 4.4407

IMAGES = 6

SPRING = -5

LCLIMB = .TRUE.
```

Bibliography

[1] Michel Armand and J-M Tarascon. “Building Better Batteries”. In: 451 (Mar. 2008), pp. 652–7.

[2] J.-M. Tarascon and Michel B. Armand. “Issues and challenges facing rechargeable lithium batteries”. In: *Nature* 414 (2001), pp. 359–367.

[3] Carine Rongeat et al. “Solid Electrolytes for Fluoride Ion Batteries: Ionic Conductivity in Polycrystalline Tysonite-Type Fluorides”. In: *ACS Applied Materials and Interfaces* 6.3 (2014). PMID: 24444763, pp. 2103–2110. DOI: 10.1021/am4052188. eprint: https://doi.org/10.1021/am4052188. URL: https://doi.org/10.1021/am4052188.

[4] Windischbacher Andreas. *Theoretische Characterisierung der Defect-Chemie von Lanthan-Perovskit-Strukturen*. 2017.

[5] Lucjan Piela. “Chapter 2 - Schroedinger Equation”. In: *Ideas of Quantum Chemistry (Second Edition)*. Ed. by Lucjan Piela. Second Edition. Oxford: Elsevier, 2014, pp. 61–101. ISBN: 978-0-444-59436-5. DOI: https://doi.org/10.1016/B978-0-444-59436-5.00002-7. URL: http://www.sciencedirect.com/science/article/pii/B9780444594365000027.

[6] Daniel Pueschner. *Quantitative Rechenverfahren der Theoretischen Chemie*. Springer Spektrum, 2017.

[7] G. Kresse and J. Hafner. “Ab initio molecular dynamics for liquid metals”. In: *Phys. Rev. B* 47 (1 Jan. 1993), pp. 558–561. DOI: 10.1103/PhysRevB.47.558. URL: https://link.aps.org/doi/10.1103/PhysRevB.47.558.

[8] G. Kresse and J. Furthmueller. “Efficiency of ab-initio total energy calculations for metals and semiconductors using a plane-wave basis set”. In: *Computational Materials Science* 6.1 (1996), pp. 15–50. ISSN: 0927-0256. DOI: https://doi.org/10.1016/0927-0256(96)00008-0. URL: http://www.sciencedirect.com/science/article/pii/0927025696000080.

[9] G. Kresse and J. Furthmueller. “Efficient iterative schemes for ab initio total-energy calculations using a plane-wave basis set”. In: *Phys. Rev. B* 54 (16 Oct. 1996), pp. 11169–11186. DOI: 10.1103/PhysRevB.54.11169. URL: https://link.aps.org/doi/10.1103/PhysRevB.54.11169.

[10] *Energy cut-off ENCUT, and FFT-mesh*. Accessed: 27.06.2018. URL: http://cms.mpi.univie.ac.at/vasp/guide/node170.html.

[11] John P. Perdew, Kieron Burke, and Matthias Ernzerhof. “Generalized Gradient Approximation Made Simple”. In: *Phys. Rev. Lett.* 77 (18 Oct. 1996), pp. 3865–3868. DOI: 10.1103/PhysRevLett.77.3865. URL: https://link.aps.org/doi/10.1103/PhysRevLett.77.3865.

[12] P.E.Bloechl. “Projector augmented-wave method”. In: *Physical Review B* 50 (1994), p. 17953.

[13] G.Kresse J. Joubert. “From ultrasoft pseudopotentials to the projector augmented wave method”. In: *Physical Review B* 59 (1999), p. 1758.

[14] Graeme Henkelman, Blas P. Uberuaga, and Hannes Jonsson. “A climbing image nudged elastic band method for finding saddle points and minimum energy paths”. In: *The Journal of Chemical Physics* 113.22 (2000), pp. 9901–9904. DOI: 10.1063/1.1329672. eprint: https://doi.org/10.1063/1.1329672. URL: https://doi.org/10.1063/1.1329672.

[15] Graeme Henkelman and Hannes Jonsson. “Improved Tangent Estimate in the Nudged Elastic Band Method for Finding Minimum Energy Paths and Saddle Points”. In: 113 (Dec. 2000), pp. 9978–9985.

[16] C. David Sherrill. *Computing Thermodynamic Quantities*. Accessed: 27.8.2018. URL: http://vergil.chemistry.gatech.edu/courses/chem6485/pdf/thermo.pdf.

[17] Z.-L. Lv et al. “Electronic and elastic properties of BaLiF3 with pressure effects: First-principles study”. In: *Physica Status Solidi (B) Basic Research* 253.9 (2016). cited By 4, pp. 1788–1794. DOI: 10.1002/pssb.201600094. URL: https://www.scopus.com/inward/record.uri?eid=2-s2.0-84969961843&doi=10.1002%2fpssb.201600094&partnerID=40&md5=1b9edcabd9f7d60c8a027df68f01bfe5.

[18] R.A. Jackson, M.E.G. Valerio, and J.F. De Lima. “Computer modelling of BaLiF3: I. Interionic potentials and intrinsic defects”. In: *Journal of Physics Condensed Matter* 8.50 (1996). cited By 25, pp. 10931–10937. DOI: 10.1088/0953-8984/8/50/019.

[19] A. Boumriche et al. “Structure and dynamics of the inverted perovskite BaLiF3”. In: *Solid State Communications* 91.2 (1994). cited By 27, pp. 125–128. DOI: 10.1016/0038-1098(94)90268-2.

[20] *Recommended PAW potentials for DFT calculations using vasp.5.2*. Accessed: 27.8.2018. URL: http://cms.mpi.univie.ac.at/vasp/vasp/Recommended_PAW_potentials_DFT_calculations_using_vasp_5_2.html.

[21] *Accurate bulk relaxations with internal parameters (one)*. Accessed: 27.8.2018. URL: https://cms.mpi.univie.ac.at/vasp/vasp/Accurate_bulk_relaxations_with_internal_parameters_one.html.

[22] *The INCAR File*. Accessed: 28.06.2018, and follow up pages for each tag. URL: http://cms.mpi.univie.ac.at/vasp/guide/node91.html.

[23] *IVDW, approximate vdW correction methods*. Accessed: 23.08.2018. URL: https://cms.mpi.univie.ac.at/vasp/vasp/IVDW_approximate_vdW_correction_methods.html.

[24] *DFT-D3 method*. Accessed: 23.08.2018. URL: https://cms.mpi.univie.ac.at/vasp/vasp/DFT_D3_method.html.

[25] *DFT-D2 method*. Accessed: 23.08.2018. URL: https://cms.mpi.univie.ac.at/wiki/index.php/DFT-D2.

[26] Nobuhiro Ogihara et al. "Impedance Spectroscopy Characterization of Porous Electrodes under Different Electrode Thickness Using a Symmetric Cell for High-Performance Lithium-Ion Batteries". In: *The Journal of Physical Chemistry C* 119.9 (2015), pp. 4612–4619. DOI: 10.1021/jp512564f. eprint: https://doi.org/10.1021/jp512564f. URL: https://doi.org/10.1021/jp512564f.

[27] Bernard A. Boukamp. "Electrochemical impedance spectroscopy in solid state ionics: recent advances". In: *Solid State Ionics* 169.1 (2004). Proceedings of the Annual Meeting of International Society of Electrochemistry, pp. 65–73. ISSN: 0167-2738. DOI: https://doi.org/10.1016/j.ssi.2003.07.00. URL: http://www.sciencedirect.com/science/article/pii/S016727380400058X.

[28] Stefan Breuer et al. "Fluorine Translational Anion Dynamics in Nanocrystalline Ceramics: SrF2-YF3 Solid Solutions". In: 8 (Mar. 2018), p. 122.

[29] Welch Ludekens. *Reactions between metal oxides and fluorides: some new double-fluoride structures of type A B F3*. 1952.

[30] B.G. Yalcin, B. Salmankurt, and S. Duman. "Investigation of structural, mechanical, electronic, optical, and dynamical properties of cubic BaLiF3, BaLiH3, and SrLiH3". In: *Materials Research Express* 3.3 (2016). cited By 11. DOI: 10.1088/2053-1591/3/3/036301.

[31] S.A. Korba et al. "First principles calculations of structural, electronic and optical properties of BaLiF3". In: *Computational Materials Science* 44.4 (2009). cited By 36, pp. 1265–1271. DOI: 10.1016/j.commatsci.2008.08.012.

[32] Dirk Zahn, Sven Herrmann, and Paul Heitjans. "On the mechanisms of ionic conductivity in BaLiF3: A molecular dynamics study". In: 13 (Nov. 2011), pp. 21492–5.

[33] Anton Bochakrev et al. "Ab initio study of Cu impurity diffusion in bulk TiN". In: 94 (Sept. 2016), p. 104303.

[34] A. Duevel et al. "Access to metastable complex ion conductors viamechanosynthesis: preparation, microstructure and conductivity of (Ba,Sr)LiF3 with inverse perovskite structure". In: *J. Mater. Chem.* 21 (2011), pp. 6238–6250. ISSN: 17. DOI: 10.1039/C0JM03439H. URL: http://dx.doi.org/10.1039/C0JM03439H.

[35] A. Duevel et al. "Mechanosynthesized nanocrystalline BaLiF3: The impact of grain boundaries and structural disorder on ionic transport". In: *Physical chemistry, chemical physics* 12 (2010), pp. 11251–11262. ISSN: 1463-9076. DOI: 10.1039/C004530F.

[36] A. Duvel et al. "Ion conduction and dynamics in mechanosynthesized nanocrystalline BaLiF3". In: *Solid State Ionics* 184.1 (2011). Exploring Chemical and Structural Complexity of Novel Ion Conductors, pp. 65–69. ISSN: 0167-2738. DOI: https://doi.org/10.1016/j.ssi.2010.08.025. URL: http://www.sciencedirect.com/science/article/pii/S0167273810004893.